Ultrafast electron and lattice dynamics at potassium-covered Cu(111) surfaces

Kazuya Watanabe

Department of Chemistry, Graduate School of Science, Kyoto University, Kyoto 606-8502, Japan
and PRESTO, JST, 4-1-8 Honcho Kawaguchi, Saitama 332-0012, Japan

Ken-ichi Inoue and Ikuyo F. Nakai

Department of Chemistry, Graduate School of Science, Kyoto University, Kyoto 606-8502, Japan

Masanori Fuyuki[*]

The Graduate University for Advanced Studies, Hayama, Kanagawa 240-0193, Japan

Yoshiyasu Matsumoto[†]

Department of Chemistry, Graduate School of Science, Kyoto University, Kyoto 606-8502, Japan;
The Graduate University for Advanced Studies, Hayama, Kanagawa 240-0193, Japan;
and Institute for Molecular Science, Okazaki, Aichi 444-8585, Japan
(Received 18 February 2009; revised manuscript received 3 July 2009; published 4 August 2009)

Electron and coherent phonon dynamics at potassium-covered Cu(111) surfaces have been studied by using femtosecond time-resolved second-harmonic generation (TRSHG). At the coverages from 0.22 to 0.35 monolayer (ML), TRSHG traces show the oscillatory component with a frequency of 3.05 ± 0.05 THz. The amplitude of this component decreases as coverage increases higher than ~0.35 ML, whereas another oscillating component with a frequency of 1.26 ± 0.03 THz grows. Both components are ascribed to K-Cu stretching motion. The spectral changes with coverage suggest that the overlayer structure varies with lateral compression. The fast transient peak in TRSHG traces at around zero delay changes its sign from negative to positive when coverage exceeds ~0.22 ML. Since the quantum-well state (QWS) is partly filled at around this coverage, electrons in the QWS are principally responsible for the transition of the electronic response. Furthermore, the excitation photon energy dependence of TRSHG traces indicates that the excitation of substrate d-band electrons, giving rise to rapid charge fluctuations in the QWS, generates the coherent K-Cu stretching vibration. Consequently, the QWS plays a major role in the electronic and nuclear dynamics induced by pump pulses at $h\nu=2.2$ eV.

I. INTRODUCTION

Electron confinement is one of the central issues in nanoscale physics and chemistry. Even at a metal surface, electrons can be trapped in a potential well between the surface and the vacuum if the metal has a local band gap in the direction normal to the surface. This electron confinement gives rise to quantum-well states (QWSs) that form two-dimensional (2D) electron gases. The interactions between quasiparticles in the QWS, different from those of bulk metals, strongly influence physical and chemical properties of metal surfaces. Therefore, knowledge of QWSs on metal surfaces has a great importance in surface science and nanotechnology.

QWSs at alkali-metal overlayers on metals have been extensively studied experimentally[1–11] and theoretically.[12–21] A metallic alkali monolayer introduces new surface electronic bands. The bands most relevant to bonding at the alkali overlayer are those originating from the free-electron-like bands of a freestanding close-packed alkali-atom monolayer: the s-like lowest and the p-like second lowest bands.[22] These bands maintain the integrity when the monolayer is placed at a metal surface. On a metal substrate with an s,p-inverted projected band gap such as Cu(111), a two-dimensional potential well is formed between the substrate and the vacuum barrier. Since the p-like band is located in the L band gap of

Cu(111), it turns out to be a QWS; the wave function is strongly localized at the surface. The QWS band, unoccupied in low coverages, is stabilized and partly filled as alkali coverage increases. In contrast, because the s-like band is located below the lower edge of the L band gap, this band becomes a surface resonance and is denoted as an overlayer resonance (OR). In addition to these bands, a series of unoccupied image potential states (IPSs) is pinned to the vacuum level.

Since these electronic states have wave functions confined more or less at the surface where alkali atoms are located, charge-density fluctuations in the surface bands strongly affect the vibrational motions of alkali atoms. This was demonstrated in recent theoretical studies;[16,17] holes generated at the occupied QWS of Na/Cu(111) preferentially decay by inelastic electron-phonon scattering. This strong electron-phonon coupling was also noted in other metallic quantum well systems: Ag/V(100) (Ref. 23) and Ag/Fe(100).[24] Thus, electron-phonon coupling at the metallic quantum well systems plays an important role in the temporal evolution of quasiparticles and nuclear dynamics at the surfaces. The electron-phonon coupling in the QWSs has been mainly explored through analysis of spectral linewidths in photoemission and scanning tunneling spectroscopy.[4,15–18,20,21] However, little attention has been paid on how the vibrational

modes of alkali atoms are excited and decay under the presence of the QWS.

Femtosecond time-resolved second-harmonic generation (TRSHG) has been proved to be a powerful technique to explore electron-phonon coupling at surfaces.[25–27] Recently, we have applied this technique to alkali-covered metal surfaces.[28–34] When the duration of pump-laser pulses irradiated onto a surface is shorter than a period of adsorbate vibration, adsorbates start vibrating coherently because of an impulsive force. The coherent nuclear motions can be monitored in terms of oscillatory modulations of the second-harmonic (SH) intensity of probe pulses as a function of pump-probe delay. Thus, the oscillatory features in the TR-SHG traces provide information on the vibrational frequency and the dephasing rate of the vibrational wavepacket created at the surface; the dephasing rate includes contributions from population decay and pure dephasing rates.

Previously we reported the excitation mechanism and the decay dynamics of coherent surface phonons at Na-covered Cu(111) surfaces.[34] At the saturation coverage, sodium atoms adsorb to form the commensurate hexagonal structure, $(3/2 \times 3/2)$.[14,35] This superstructure has two distinguishable adsorption sites: threefold hollow and distorted hollow sites. Theoretical calculations predicted that the Na-Cu stretching mode is strongly mixed with substrate phonon modes at the saturation coverage.[36] Thus, a wavepacket created along the Na-Cu stretching coordinate is expected to decay rapidly to the substrate phonon modes. This was indeed confirmed in the TRSHG measurements.[34]

Potassium adatoms also form hexagonal structures on Cu(111). However, they are mostly incommensurate to the substrate lattice. Low-energy electron-diffraction (LEED) measurements showed that K-K spacing decreases as coverage increases, while overlayers at low temperature keep the orientationally ordered hexagonal structure.[37] Thus, the adsorption sites are largely inhomogeneous. Consequently, it is interesting to investigate how the inhomogeneity in adsorption sites influences the decay behavior of coherently excited K-Cu stretching vibration in comparison with Na/Cu(111).

In this paper, we describe the dynamics of electrons and coherent phonons at potassium-covered Cu(111) surfaces. We show that electronic and nuclear responses to a femtosecond laser pulse strongly depend on the energy of the QWS band with respect to the Fermi level E_F. We also discuss an important role of the QWS band in excitation of the coherent surface phonons.

II. METHODS

The experiments were carried out in an ultrahigh vacuum chamber equipped with various instruments for conventional surface science techniques: Auger electron spectroscopy, low-energy electron diffraction, and temperature-programmed desorption. A Cu(111) surface was cleaned by repeated cycles of sputtering and annealing. Potassium atoms from a degassed alkali dispenser (SAES Getters) were deposited on the clean Cu(111) surface at 90–110 K. Potassium coverage θ_K was monitored in terms of the ratio of Auger electron emission intensity at 248 eV (K:LMM) to that at

915 eV (Cu:LMM) as a function of deposition time t_K.

We used various kinds of light pulses in TRSHG measurements as pump and/or probe pulses. The second-harmonic output of a Ti:sapphire regenerative amplifier ($\lambda = 400$ nm, pulse width=130 fs, and repetition rate=1 kHz) pumped two sets of homebuilt noncollinear optical parametric amplifiers (NOPAs). The duration of NOPA output pulses was 25–35 fs and the photon energy of NOPAs was tuned from 2.0 to 2.5 eV independently. The fundamental output of the regenerative amplifier ($\lambda = 800$ nm) was also used as pump and/or probe pulses. Since a pulse width of 130 fs was too long for pump, the fundamental output pulses were compressed as follows: the output pulse (0.8 mJ) was focused with a quartz lens (focal length=1 m) into a cylindrical tube filled with Kr gas (~2 atm). This procedure broadened the spectral width of output pulses as a result of nonlinear effects. Then, the pulse was compressed with the aid of additional multiple reflections between a pair of negative group-velocity dispersion mirrors. The compressed pulse width was estimated to be 35 fs by using autocorrelation measurements.

The procedure for TRSHG measurements is almost the same as reported previously.[32–34] Pump and probe pulses with p polarization were focused onto the sample surface at an angle-of-incidence of ~70°. Pump pulses were alternately blocked with an optical chopper for phase-sensitive detection of pump-induced changes in the surface SH intensity of probe pulses. Transient changes in SH intensity $\Delta I_{SH}(t)$ are defined as $\Delta I_{SH}(t) = [I_{SH}(t) - I_{SH}^0(t)]/I_{SH}^0(t)$, where $I_{SH}(t)$ and $I_{SH}^0(t)$ are SH intensities at a pump-probe delay-time t with and without pump pulses, respectively. All the measurements were carried out at a sample temperature of 90 ± 5 K.

The potassium coverage dependence of TRSHG traces was measured with compressed 800-nm pulses as a probe and the NOPA output (centered at $\lambda = 565$ nm) as a pump. The excitation photon energy dependence of TRSHG traces was mainly studied by using the two NOPAs. The first NOPA used as a probe was fixed at $h\nu = 2.2$ eV, while the second NOPA as a pump was tuned from $h\nu = 2.0$ to 2.4 eV. The pump photon energy range was extended to 1.55 eV by using compressed 800-nm pulses. For estimation of pump fluence at the sample surface, pump pulses were reflected off with a mirror outside the chamber and the spot profile of pump pulses was observed with a charge-coupled device beam profiler. A great care was taken to set the distance from the steering mirror to the beam profiler to be the same as that from the mirror to the sample surface. The estimated pump fluence at the sample surface was typically 2–3 mJ/cm^2.

Total energies were calculated with the density functional theory (DFT) method as a function of displacement of a potassium overlayer from a Cu surface. The CASTEP package in Materials Studio (Accelrys Inc.) was used for the DFT calculations with a plane-wave basis set under periodic boundary conditions.[38,39] Ultrasoft pseudopotentials[40] were used for the effective potential of ions. The nonspin polarized version of the generalized gradient approximation (GGA-PBE) (Ref. 41) was employed in calculations of total electron energy.

Potassium overlayers on Cu(111) were modeled with supercells composed of seven layers of fcc-(111) stacked copper atoms, a potassium overlayer, and 20-Å thick vacuum.
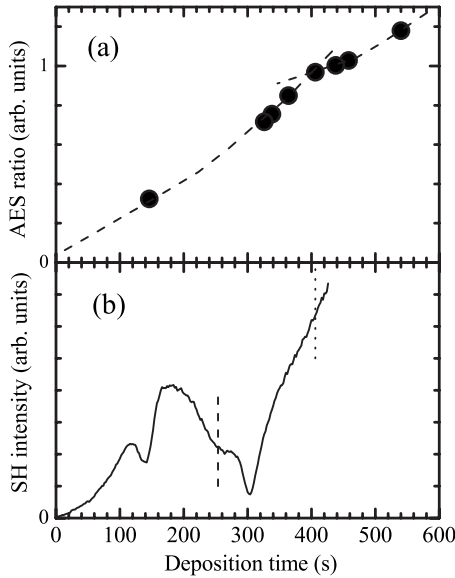
FIG. 1. (a) Ratio of Auger peak intensity at 248 eV (K:LMM) to that at 915 eV (Cu:LMM) as a function of potassium deposition time. Dashed curves are drawn as a guide to the eyes. A bend at ~410 s indicates that the first layer is saturated. (b) SH intensity from Cu(111) as a function of potassium deposition time. The center wavelength of incident beam is 800 nm. Dashed and dotted lines denote potassium coverages of 0.25 and 0.40 ML, respectively.

First, we calculated the minimum total energy by relaxing the potassium overlayer and two topmost Cu layers in geometry optimization procedures. Then, the total energy was calculated as a function of displacement of the overlayer from the copper surface while the structure of the Cu slab was kept frozen. The energy difference between those calculated with and without geometry optimization was estimated to be less than 3%. The use of the ultrasoft pseudopotentials enabled good convergence at a plane-wave energy cutoff of 270 eV. Brillouin zones of supercells, (2×2) and $(3/2 \times 3/2)$, were sampled by $(5 \times 5 \times 1)$ and $(3 \times 3 \times 1)$ Monkhorst-Pack grids,[42] respectively. Finite temperature smearing of $k_B T = 0.3$ eV was used to diminish the number of k points necessary for convergence.

III. SURFACE PHONON STRUCTURE AND DECAY DYNAMICS

A. Potassium coverage and overlayer structure

Auger peak intensity ratios, K(248 eV)/Cu(915 eV), are plotted in Fig. 1(a) as a function of deposition time t_K. The growth curve of ratio has a bend at $t_K \sim 410$ s, indicating that the first layer is saturated at this deposition time and the second layer grows in $t_K > 410$ s. The saturation coverage was tentatively taken to be 0.40 ML [1 ML is the atomic density of clean Cu(111) surface, 1.8×10^{15} cm^{-2}] as in the LEED study by Fan and Ingantiev.[37] Then, we determined all coverages used in the measurements with t_K, assuming that the deposition rate is constant. As expected, a clear (2×2) LEED pattern was observed at $\theta_K = 0.25$ ML. This implies that this calibration method gives reasonably accurate potas-
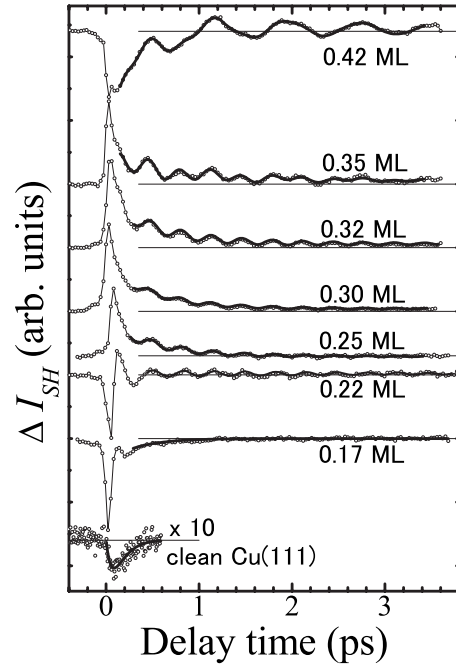
FIG. 2. Coverage dependence of TRSHG traces for potassium-covered Cu(111) surfaces measured with pump pulses at $h\nu$ =2.20 eV and probe pulses at $h\nu$=1.55 eV. Coverages are indicated in the figure. Open circles connected with thin lines are observed results and thick solid curves are fitting results obtained with Eq. (1). Fitting parameters are listed in Table I. The bottom is a TRSHG trace for clean Cu(111) (open circles) and a nonlinear least-square fitting result with a double exponential function (solid curve).

sium coverage. As θ_K increased over $\theta_K = 0.25$ ML, the (2×2) spots split into two and the separation between the spots increased with coverage up to the first layer saturation. This is due to formation of orientationally ordered incommensurate hexagonal structures of potassium overlayers.[37]

Figure 1(b) shows how the SH intensity of 800-nm ($h\nu = 1.55$ eV) photons changes as a function of deposition time. As in other alkali-metal adsorption systems,[30–34,43–46] alkali deposition enhances markedly SHG conversion efficiency. The SH intensity at $\theta_K = 0.40$ ML is higher than that at $\theta_K = 0$ by a factor of ~70. Thus, transitions between electronic states introduced by the alkali overlayer dominate for generating SH signals over those between substrate bands. Since the metallic OR band is a primary source of excess electrons at the surface, the transitions from the OR band should play a major role in enhancing SH conversion efficiency. In addition, since the QWS band is partly filled at $\theta_K \geq 0.25$ ML, electrons in the QWS band also enhance SH generation efficiency. Therefore, the peaks in Fig. 1(b) could be due to resonant or near-resonant transitions in which the surface localized bands, OR, QWS, and IPSs, are involved.

B. Coverage dependence of TRSHG traces

Figure 2 shows typical TRSHG traces at various coverages. The center wavelength of pump pulses was 565 nm ($h\nu = 2.20$ eV), while that of probe pulses was 800 nm ($h\nu$

TABLE I. Parameters in Eq. (1) obtained by analysis of TRSHG traces in Fig. 2 by using linear prediction singular value decomposition.

θ_K (ML)	$\tau_1^{(p)}$ (ps)	ω_1 (THz)	ϕ_1 (degree)	$\tau_2^{(p)}$ (ps)	ω_2 (THz)	ϕ_2 (degree)	$\tau_1^{(e)}$ (ps)
0.17							0.33
0.22	2.34	3.03	−11				
0.25	1.27	3.02	11				0.51
0.30	1.46	3.02	13				0.50
0.32	1.72	3.06	−6				0.53
0.35	1.23	3.03	37	2.28	1.28	15	0.67
0.42	0.89	3.00	6	3.12	1.27	4	0.32

=1.55 eV). The TRSHG trace from a clean Cu(111) surface has a very weak negative peak at $t\sim100$ fs. This time profile reflects an electron temperature rise and subsequent decay in the copper substrate.[47,48] This is fitted well with a negative double exponential function with a rise time of 80 fs and a decay time of 94 fs.

Potassium deposition appreciably altered the transient SH response. TRSHG traces from alkali-covered surfaces are contributed by population changes in surface and substrate electronic bands as well as coherent nuclear vibrations at the surface.[32–34,49] The former gives rise to a spike at $t\sim0$ ps and nonoscillatory decaying components extending to $t\sim2$ ps, while the latter emerges as damped oscillatory components that are appreciable only at $\theta_K \geq 0.22$ ML. Here, we first focus on the nuclear response and discuss the electronic response in Sec. IV.

The TRSHG traces in $t\geq200$ fs were analyzed with linear prediction singular value decomposition[32,50] under the assumption that the trace is a superposition of damped cosinusoidals and exponential decay functions,

$$\Delta I_{SH}(t) = \sum_i A_i \exp(-t/\tau_i^{(p)})\cos(\omega_i t + \phi_i)$$

$$+ \sum_j B_j \exp(-t/\tau_j^{(e)}). \qquad (1)$$

Here, the i-th damped oscillatory component is characterized with the frequency ω_i, the initial phase ϕ_i, and the dephasing time $\tau_i^{(p)}$, and the j-th exponential decay component is characterized with the energy relaxation-time $\tau_i^{(e)}$. The obtained parameters are listed in Table I, where minor components with a relative amplitude less than 10% are omitted. The fitting quality with these parameters is excellent as shown in Fig. 2.

C. Phonon spectra

Phonon spectra were obtained by Fourier transformation of the time-domain data in $t\geq200$ fs after the background components were subtracted. Each phonon spectrum at $0.20 < \theta_K < 0.35$ ML in Fig. 3 shows a single peak at 3.05 ± 0.05 THz. As θ_K exceeds 0.35 ML, a new peak appears at 1.26 ± 0.03 THz. The relative amplitudes of the two components are plotted in Fig. 4 as a function of θ_K. The

lower-frequency peak increases in its relative amplitude with θ_K and becomes dominant at $\theta_K > 0.38$ ML. From now on, the higher-frequency component at ~3.1 THz is denoted as α and the lower-frequency component at ~1.3 THz as β.

Previous studies of high-resolution electron energy loss spectroscopy (HREELS) reported a loss peak at 13 meV (3.1 THz) (Refs. 51 and 52); this peak was attributed to the K-Cu stretching mode. The loss peak shows little energy shift up to $\theta_K\sim0.3$ ML. The frequency and its coverage dependence of α component observed in the current study are consistent with the HREELS results.

DFT calculations also support this assignment. Figure 5 shows the total energy of Cu(111)-(2×2)-K calculated as a function of displacement of a potassium layer from the copper surface. Fitting the calculated results with a Morse function, we obtained a vibrational frequency of 3.6 THz; this is close to the observed frequency of 3.05 ± 0.05 THz. Since
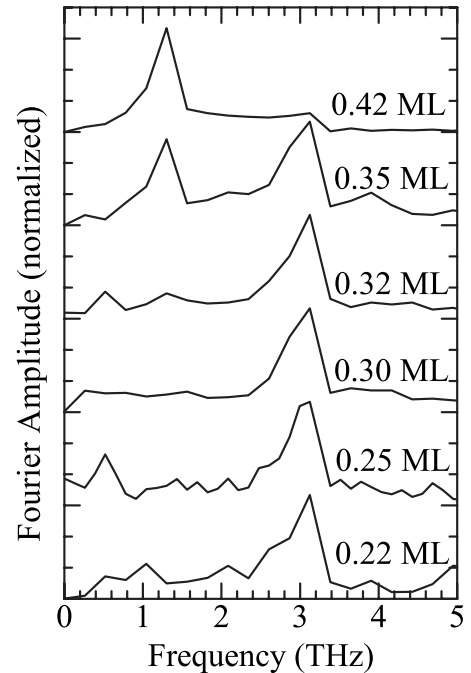
FIG. 3. Fourier amplitude spectra of the oscillatory components in TRSHG signals ($t > 200$ fs). Coverages are indicated in the figure. The amplitudes are normalized at the highest peak in each spectrum.
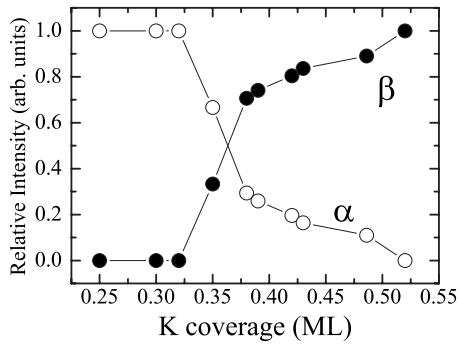
FIG. 4. Coverage dependence of the relative peak height of the α (open circles) and β (filled circles) components in the Fourier amplitude spectra in Fig. 3.

the substrate lattice is frozen in the calculations, the consistency between the calculated and observed frequencies implies that the K-Cu stretching mode is well represented by oscillating motion of potassium; Cu phonon modes would be little involved in the stretching mode.

Next, let us focus on the β component observed at $\theta_K \geq 0.35$ ML. In the previous HREELS studies, the β component was not observed.[51,52] This may be partly due to weak HREELS signals at high coverages, because a dynamic charge appreciably decreases as a result of large charge redistribution in alkali atoms.[51,52]

The frequencies of adsorbate vibrational modes usually shift with coverage. As for alkali adsorbates, the continuous coverage-dependent frequency shifts in the alkali stretching mode were observed in the HREELS studies of Cs/Ru(0001) (Ref. 53) and K/Pt(111) (Ref. 54) at room temperature. A similar tendency was found by the TRSHG study of Cs/Pt(111) at 110 K.[32] The shifts can be explained in part by dipole coupling among alkali atoms. In contrast, the phonon spectra in Fig. 3 shows that the frequency change with coverage is not gradual but abrupt. Furthermore, the frequencies of both the α and β components stay constant in the entire coverage range observed. Thus, the coverage dependence of vibrational frequencies in the current study cannot be accounted for by the dipole-dipole coupling among adsorbates.
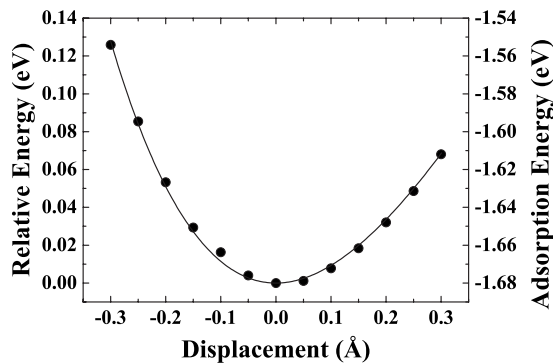
FIG. 5. Total energy of Cu(111)-(2×2)K as a function of displacement of the potassium layer from the copper surface. The right vertical axis indicates the energy scale for adsorption energy per potassium atom. The solid line is a fitting result by a Morse function. The K-Cu distance at the energy minimum is 2.9 Å.

Since the β component starts growing when the potassium overlayer is close to the saturation, the β component could be due to the second-layer growth. However, as shown in Fig. 4, the β component is much stronger than the α component already at $\theta_K \sim 0.40$ ML where the surface area covered with potassium atoms in the second layer is negligibly small. In addition, if the β component were due to the formation of the second layer, the amplitude of β component should increase with coverage in comparison with the nonoscillatory backgrounds that are almost independent of coverage. However, this was not observed. Therefore, the β component does not likely originate in the formation of the second layer.

Frequencies of adsorbate vibrational modes depend on adsorption structures and sites. For example, when a potassium overlayer on Pt(111) changes its superstructure from (2×2) to $(\sqrt{3} \times \sqrt{3})$R30°, the frequency of a K-Pt stretching-mode shifts discontinuously.[33] Thus, the abrupt frequency change could be explained by a change in the overlayer structure. However, no abrupt changes have been reported in the adsorption structure of potassium on Cu(111). According to the detailed LEED analysis,[37] potassium overlayers form mostly incommensurate, but orientationally ordered hexagonal structures at $\theta_K > 0.14$ ML, while the K-K spacing decreases with increase in coverage. Therefore, it is difficult to account for the abrupt frequency change in terms of the gradual coverage-dependent compression of hexagonal structure.

Compression of the planar hexagonal structure makes mutual repulsion between adatoms appreciable. This may destabilize the planar structure and convert into a corrugated one. For example, Monte Carlo simulations of potassium adsorption on Cu(111) showed that an overlayer at 80 K becomes corrugated even at $\theta_K = 0.25$ ML, where potassium forms a commensurate (2×2) structure, and tends to form a bilayer.[55] This is a manifestation of the repulsive interaction between potassium adatoms.

DFT calculations provide a clue for appearance of the β component. To examine how the mutual repulsion affects the overlayer structure, we chose a $(3/2 \times 3/2)$-K superstructure. This superstructure gives the highest coverage among those of commensurate structures we can handle with our limited computer resource. The coverage is 0.44 ML, slightly higher than the tentatively determined saturation coverage of 0.4 ML. The K-K nearest-neighbor distance in this overlayer is 3.91 Å; this is by 11% smaller than the smallest lattice parameter for the potassium overlayer observed in the LEED measurements, 4.4 Å.[37] We calculated total electron energy as a function of displacement of the potassium overlayer from the surface. The vibrational frequency obtained from the fitting with a Morse function is 2.8 THz, consistent with that of the α component.

Although the planar structure is still stablest at $\theta_K = 0.44$ ML, we found a corrugated metastable structure. We took an overlayer structure model depicted in Fig. 6(a). In this structure, potassium atoms on atop sites are displaced along the surface normal, while those on bridge sites are kept at the same position as in the optimized $(3/2 \times 3/2)$ planar structure. In Fig. 6(b), the total energy is plotted as a function of displacement of potassium atoms on atop sites. It clearly shows that a local minimum is located at 3.1 Å away from
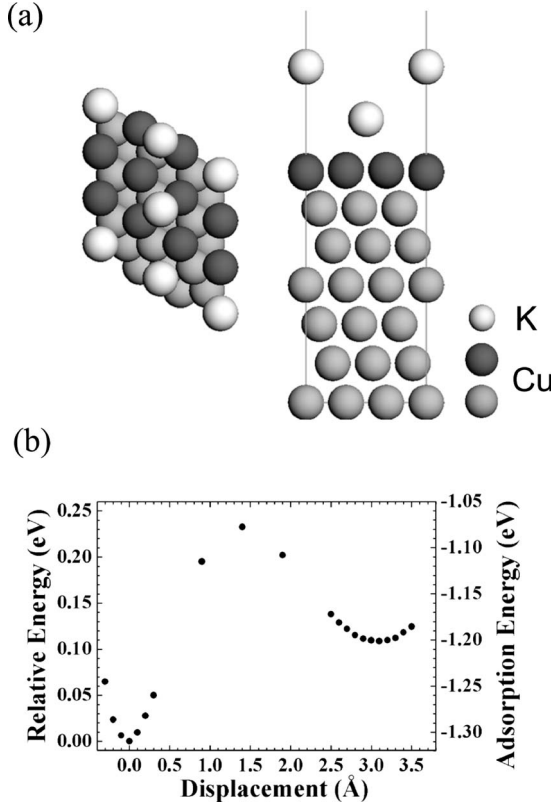
FIG. 6. (a) The structure used for calculations of total energy of Cu(111)-(3/2×3/2)-K. Potassium atoms on atop sites are displaced along the surface normal, while those on bridge sites are fixed at the displacement given by geometry optimization of the (3/2×3/2) planar structure. (b) Total energy is plotted as a function of displacement of potassium atoms on atop sites. The right vertical axis indicates the energy scale for adsorption energy per potassium atom.

the equilibrium position of the planar structure. This bilayer structure is metastable; the energy is higher than that of the planar structure by 0.12 eV per potassium atom. Because the barrier height from the metastable configuration to the planar one is 0.12 eV, potassium adsorbates can form this metastable bilayer structure at a sample temperature of 90 K. Since atop potassium atoms are much away from the surface in the bilayer structure, the interaction between the copper surface and the bilayer becomes weaker than the planar one; this gives rise to a shallower potential-energy curve along the surface normal. In fact, the vibrational frequency of bilayer in Fig. 6 was found from calculations to be 2.7 THz, lower than that of planar (2×2)-K, 3.6 THz. When bridge potassium atoms are displaced instead of atop atoms, DFT calculations also showed a local minimum in total energy at around 3 Å. Therefore, we propose that the lateral compression with increase in coverage leads to form two domains near the saturation coverage: the planar domain with a stretching frequency of ~3.1 THz and the bilayer one with a frequency of ~1.3 THz.

D. Decay of vibrational coherence

As in Table I, the decay times of α component range from 1.2 to 1.7 ps at $0.25 \leq \theta_K \leq 0.35$ ML and those of β compo-

nent are even longer. These are sevenfold longer than the decay time of Na/Cu(111) estimated from the full-width-at-half-maximum (FWHM) of the Na-Cu stretching band in the Fourier spectrum of the TRSHG trace at the saturation coverage.[34] According to the theoretical calculations by Borisova *et al.*,[36] the Na-Cu stretching mode is strongly mixed with Cu substrate phonon modes. In addition, because of two adsorption sites, threefold hollow and distorted hollow sites, the local density of phonon bands with the stretching-mode character is distributed over the wide frequency range from 2.3 to 6 THz. Thus, the fast decay dynamics can be due to rapid dephasing of a wavepacket along the Na-Cu stretching coordinate prepared by coherent excitation of the inhomogeneously distributed surface phonon bands.

In contrast, the phonon band of the K-Cu stretching mode in Fig. 3 is much narrower, indicating that the K-Cu stretching mode is not mixed well with Cu surface phonon modes. In addition, although potassium atoms adsorb in various adsorption sites as a result of the incommensurate structures, the inhomogeneity in adsorption sites does not contribute to the phonon bandwidth. Thus, the rapid dephasing of wavepacket observed in Na/Cu(111) does not take place.

One of possible decay mechanisms is energy relaxation by emission of phonons into the substrate. In the elastic continuum model for ordered commensurate adsorbate layers,[56] a surface vibrational damping time is given by $\rho c_L / m \omega_0^2 n_a$, where m is the adsorbate mass, n_a is the adsorbate density, ω_0 is the vibrational frequency, ρ is the substrate mass density, and c_L is the longitudinal sound velocity of the substrate. From this equation, we estimated the vibrational damping time for the stretching mode at $\theta_K = 0.25$ ML to be 0.46 ps. Because time-domain spectroscopy such as TRSHG gives the dephasing time T_2 that is twice of the population decay time T_1 if the pure dephasing time T_2^* is completely neglected,[27,57] the observed damping time to be compared with that of the elastic continuum model is 0.64 ps. Thus, the observed decay time is in relative good agreement with the theoretical estimate. In addition to the decay via one-phonon emission, electronic frictions may contribute to the decay. As we discuss in the following sections, electronic excitation and de-excitation in substrate play an important role in creation of coherent surface phonons. Thus, the reverse process, energy dissipation via electron-hole creation in the substrate, may also be partly responsible for the decay of vibrational coherence.

IV. ELECTRON DYNAMICS

Electrons excited by a pump pulse contribute to TRSHG traces particularly at a pump-probe delay of $t \sim 0$ fs. Figure 7 shows an expanded view of TRSHG traces at $-200 < t < 300$ fs at $0.16 \leq \theta_K \leq 0.27$ ML. SH intensity governed by the second-order nonlinear susceptibility, $\chi^{(2)}$, depends on various factors: the dipole matrix elements for electronic transitions, the electronic band structure, and the electron population of each band.[47,58] As noted in Sec. III A, the transitions between surface electronic bands introduced by the alkali overlayer mostly contribute to SH intensity. Thus, the
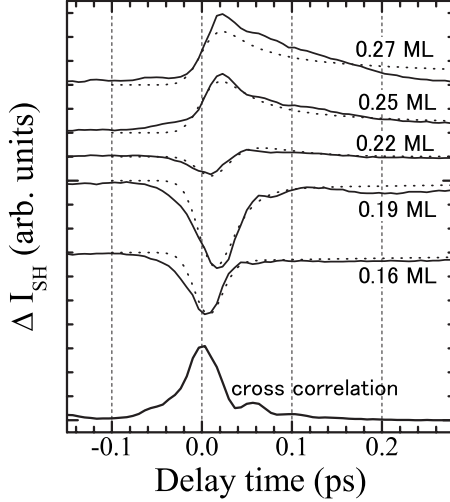
FIG. 7. Coverage dependence of TRSHG traces observed (solid curves) and simulated (dotted curves) results for K/Cu(111) near t =0. Coverages are indicated in the figure. The bottom trace is a cross correlation trace between pump and probe pulses obtained by monitoring the sum-frequency signals generated at the sample surface. The simulation results are obtained using Eq. (2) with parameters in Table II. The intensities of the simulation results are scaled to match the experimental ones.

most relevant factor to the TRSHG signals is pump-induced changes in populations of the surface electronic bands. Keeping this in mind, we simulated the coverage dependence of TRSHG traces at $-100 < t < 300$ fs as follows. We assume that the change in population of the i-th surface band $f_i(t)$ induced by the pump pulse decays exponentially, $f_i(t) = a_i \exp(-t/\tau_i)$, where a_i is the relative amplitude and τ_i is the decay time. Then, we calculated TRSHG intensity $I_{SH}(t)$ by using a convolution integral of $f_i(t)$ with Gaussian profiles of pump and probe pulses, $I_1(t)$ and $I_2(t)$, respectively,

$$I_{SH}(t) = \int_{t_1}^{t_2} I_2^2(t'-t) \left\{ \sum_i \int_{t_1}^{t} I_1(\tau) f_i(t'-\tau) d\tau \right\} dt'. \quad (2)$$

Numerical integration of Eq. (2) was carried out in the range between $t_1 = -100$ and $t_2 = 300$ fs. Typical simulated results are depicted in Fig. 7 and the parameters employed in the simulations are tabulated in Table II. The qualitative features

TABLE II. Parameters for simulations of TRSHG signals by using Eq. (2). FWHM of pump and probe pulses are assumed to be 25 and 35 fs, respectively. The values of a_i are normalized to satisfy $\Sigma_i |a_i| = 1$ for each trace.

Coverage (ML)	a_1	τ_1 (ps)	a_2	τ_2 (ps)
0.16	$-5/6$	0.005	$-1/6$	0.45
0.19	$-5/7$	0.02	$-2/7$	0.45
0.22	$-2/3$	0.02	$1/3$	0.04
0.25	$5/7$	0.04	$2/7$	0.45
0.27	$5/8$	0.04	$3/8$	0.45

of coverage dependence of TRSHG traces are well reproduced. The discrepancies between experiment and simulation are largely due to deviations of laser-pulse profiles from the Gaussian function and the oscillatory component originating in coherent nuclear vibration superimposed in the experimental data.

The electronic response in TRSHG can be classified according to the sign of the peak at $t \sim 0$ fs: the peak is negative below $\theta_K = 0.20$ ML, whereas the peak is positive above $\theta_K = 0.25$ ML. The TRSHG traces at the coverages between 0.20 and 0.25 ML, showing a differential-like profile, are in the transition from one to the other. Another striking difference between the two coverage ranges is that the oscillatory component due to the coherent K-Cu stretching mode is clearly visible at $\theta_K \geq 0.25$ ML, but not at $\theta_K < 0.20$ ML. What makes these marked differences? Note that the QWS band crosses E_F when the (2×2) structure completes, i.e., $\theta_K = 0.25$ ML.[5] Therefore, the QWS plays a decisive role in causing the differences in both electronic and nuclear responses in TRSHG.

At $\theta_K = 0.16$ ML, the TRSHG trace at $t \sim 0$ fs shows an instantaneous response; this is reproduced by a single negative component with a decay time of 5 fs.[62] As coverage increases to 0.19 ML, the negative peak grows and slightly shifts toward larger t, resulting in a decay time of 20 fs. Since the QWS band is not occupied at these coverages, this band does not contribute to the negative peaks. Instead, since the pump photon energy (2.2 ± 0.1 eV) is in near resonance with one- and two-photon transitions from the occupied OR to the QWS and to the IPSs, respectively, these transitions deplete the electron population of the OR band. Consequently, the population depletion reduces SH intensity of probe pulses, resulting in the negative peak in TRSHG traces. Although the lifetime of holes in the OR band is not known, a lifetime of ≤ 20 fs is very reasonable, since holes in the surface resonance can be filled rapidly by bulk electrons.

The differential-like profile at $0.20 < \theta_K < 0.22$ ML is reproduced by a linear combination of a negative component with $\tau = 20$ fs and a positive component with $\tau = 40$ fs. As coverage increases further ($\theta_K \geq 0.25$ ML), the positive component dominates over the negative one. Since the QWS band is located at around E_F in this coverage range,[5] electronic transitions from bulk d bands to the unoccupied s, p band enhance filling of the QWS band, resulting in increase in population in the QWS band. Thus, the extra electrons in the QWS band increase the SH intensity of probe pulses, giving rise to the positive peak in TRSHG traces.

In the entire coverage range studied, a slow decaying component with $\tau = 450$ fs contributes to the TRSHG traces, although the contribution is minor in comparison with the fast decaying components. Since this decay time is comparable to those of electrons and holes near E_F,[12] the population changes in the surface band near E_F could be responsible for the slow decay component.

V. EXCITATION MECHANISM OF COHERENT PHONONS

To clarify the electronic transitions responsible for creation of coherent surface phonons, we measured TRSHG
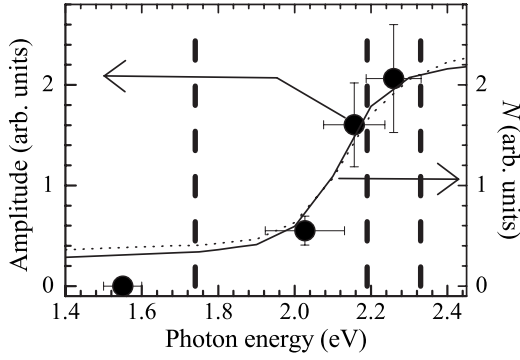
FIG. 8. Pump-photon-energy dependence of the amplitude of α component measured at $\theta_K = 0.25$ ML. The amplitude is estimated from the peak intensity in Fourier amplitude spectra of the oscillatory components in TRSHG traces. Solid and dotted curves denote the number of photo-generated carriers N estimated by using Eq. (3) with $\delta = 10$ nm (dotted) and $\delta = 1000$ nm (solid). The calculated values of N are normalized by the carrier density at a photon energy of 2.3 eV. Dashed lines denote transition energies from QWS to IPSs ($n = 1$, 2, and 3 from left to right), respectively, estimated from photoemission data (Ref. 7).

traces as a function of pump photon energy. Figure 8 shows variations in the amplitude of α component with pump photon energy, i.e., the action spectrum. Here we normalized a peak amplitude of α component by incident photon density. The amplitude of α component is not detectable at $h\nu = 1.55$ eV, but appreciable at $h\nu > 2$ eV. Although the amplitude depends on the pump photon energy, its frequency and decay time showed no definite photon energy dependence.

The transition energies between surface states estimated from two photon photoemission studies[7] are indicated in Fig. 8 as dashed lines. A resonance at 2.32 eV is due to the transition of QWS$\rightarrow n = 3$ IPS, while that at 2.19 eV is due to QWS$\rightarrow n = 2$ IPS. If these transitions were responsible for the coherent phonon excitation, the amplitude at 2.19 eV should be much larger than that at 2.32 eV, because the wave function of $n = 2$ IPS has a better spatial overlap with that of QWS than $n = 3$ IPS. However, this expectation is inconsistent with the observed action spectrum. Thus, it is unlikely that the electronic transitions between the surface states play a major role in the coherent phonon excitation.

Instead, the action spectrum in Fig. 8 rather resembles the absorption curve of bulk copper. We estimated the density of photo-excited carriers N that are generated in the Cu substrate and propagate to the surface by using the following equation:[59]

$$N = IA[1 - \exp(-\delta/D)], \quad (3)$$

where I is the incident photon number, A is the absorbance of the substrate, δ is the hot carrier mean-free path, and $D = \lambda/2\pi k$, where λ is the wavelength of pump pulses and k is the extinction coefficient of bulk copper.[60] Photon energy dependences of N for $\delta = 10$ and 1000 nm are plotted in Fig. 8, where they are normalized by the carrier density at $h\nu = 2.3$ eV and scaled to match the oscillation amplitude in the action spectrum. The action spectrum corresponds well to the

carrier density curve estimated from substrate absorption. Therefore, the substrate electronic excitation is likely responsible for the coherent phonon excitation.

A similar substrate mediated picture for coherent phonon generation has been reported for Na/Cu(111).[34] Since the emergence of α component is concomitant with stabilization of the QWS band to E_F, it is likely that the population change in the QWS band is responsible for an impulsive force along the K-Cu coordinate. One possible excitation path for generating the impulsive force is hole creation in the QWS. Electron-hole pairs are formed in the substrate by the d-band$\rightarrow s$,p-band transition, followed by subsequent Auger recombination of an electron in the QWS band with the d-band hole, resulting in creation of holes in the QWS. An appreciable coupling between the hole creation at the alkali derived QWS and surface (or interface) phonon excitation has been suggested.[17] Alternatively, hot electrons created by the d-band$\rightarrow s$,p-band transition are injected into the QWS above E_F. In either case, the rapid change in charge density at the surface could be a most likely origin for the impulsive force along the K-Cu stretching coordinate.

The initial phase of the oscillation [ϕ_i in Eq. (1)] is $8 \pm 17°$ in average; the phonon oscillation is cos-like. This indicates that coherent phonons are excited with coupling to resonantly excited charge-density fluctuations.[61] In the substrate-mediated excitation mechanism stated earlier, the initial optical transition does not couple to the nuclear motion directly, but the charge fluctuations induced by rapid charge transfer following the optical transition drive the coherent motion along the K-Cu stretching coordinate.

VI. CONCLUSION

We have studied ultrafast responses of electrons and potassium adatoms to femtosecond pump pulses by measuring transient intensity modulations in second-harmonic intensity of probe pulses. Electronic and nuclear responses to the pump pulse drastically changed at $\theta_K \sim 0.25$ ML; (1) at below $\theta_K \sim 0.25$ ML, the TRSHG trace showed a fast negative peak at $t \sim 0$ fs, almost instantaneous to the pump pulse at $h\nu = 2.2$ eV, without accompanying any oscillatory component due to coherent nuclear motions; (2) at above $\theta_K \sim 0.25$ ML, the TRSHG trace showed a positive delayed peak at $t \sim 20$ fs, followed by an oscillating component with a frequency of ~ 3 THz due to the coherent K-Cu stretching vibration. Because the unoccupied QWS band is stabilized with increase in coverage and partly filled at $\theta_K \sim 0.25$ ML, the filling of QWS is mostly responsible for the changes in electronic and nuclear responses. The action spectrum of the amplitude of the coherent phonon mode indicates that excitation of d-band electrons to the s,p band right above E_F is relevant to the creation of coherent phonons. Therefore, it is likely that the coherent phonons are excited by the substrate mediated process in which holes (electrons) transfer into occupied (unoccupied) part of the QWS band within the excitation pulse duration.

The oscillatory component due to the coherent K-Cu stretching vibration showed little coverage dependence of its frequency and decay time. However, as coverage increases to

the saturation coverage, another component with a frequency of ~1.3 THz grew, while the component with ~3 THz diminished. The low-frequency mode may be caused by a structural change of the overlayer as the hexagonal structure is compressed. In spite of the inhomogeneous adsorption sites of potassium adatoms in the incommensurate hexagonal structure, the decay times of both modes were substantially longer than that observed in the study of Na/Cu(111) at the saturation coverage. This indicates that the K-Cu stretching mode is well isolated from Cu surface phonons in comparison with the Na-Cu stretching mode.

ACKNOWLEDGMENTS

*Present address: East Tokyo Laboratory, Genesis Research Institute, Inc., 717-86 Futamata, Ichikawa, Chiba 272-0001, Japan.

†matsumoto@kuchem.kyoto-u.ac.jp

[1] S.-Å. Lindgren and L. Walldén, Phys. Rev. Lett. **59**, 3003 (1987).

[2] A. Carlsson, D. Claesson, S.-Å. Lindgren, and L. Wallden, Phys. Rev. Lett. **77**, 346 (1996).

[3] A. Carlsson, B. Hellsing, S.-Å. Lindgren, and L. Walldén, Phys. Rev. B **56**, 1593 (1997).

[4] M. Breitholtz, V. Chis, B. Hellsing, S.-Å. Lindgren, and L. Walldén, Phys. Rev. B **75**, 155403 (2007).

[5] F. Schiller, M. Corso, M. Urdanpilleta, T. Ohta, A. Bostwick, J. L. McChesney, E. Rotenberg, and J. E. Ortega, Phys. Rev. B **77**, 153410 (2008).

[6] N. Fischer, S. Schuppler, R. Fischer, T. Fauster, and W. Steinmann, Phys. Rev. B **43**, 14722 (1991).

[7] N. Fischer, S. Schuppler, R. Fischer, T. Fauster, and W. Steinmann, Phys. Rev. B **47**, 4705 (1993).

[8] N. Fischer, S. Schuppler, T. Fauster, and W. Steinmann, Surf. Sci. **314**, 89 (1994).

[9] G. Hoffmann, J. Kliewer, and R. Berndt, Phys. Rev. Lett. **87**, 176803 (2001).

[10] J. Kliewer and R. Berndt, Surf. Sci. **477**, 250 (2001).

[11] J. Kliewer and R. Berndt, Phys. Rev. B **65**, 035412 (2001).

[12] P. Echenique, R. Berndt, E. Chulkov, T. Fauster, A. Goldmann, and U. Höfer, Surf. Sci. Rep. **52**, 219 (2004).

[13] E. V. Chulkov, A. G. Borisov, J. P. Gauyacq, D. Sánchez-Portal, V. M. Silkin, V. P. Zhukov, and P. M. Echenique, Chem. Rev. (Washington, D.C.) **106**, 4160 (2006).

[14] J. M. Carlsson and B. Hellsing, Phys. Rev. B **61**, 13973 (2000).

[15] B. Hellsing, J. Carlsson, L. Walldén, and S.-Å. Lindgren, Phys. Rev. B **61**, 2343 (2000).

[16] B. Hellsing, A. Eiguren, and E. V. Chulkov, J. Phys.: Condens. Matter **14**, 5959 (2002).

[17] E. V. Chulkov, J. Kliewer, R. Berndt, V. M. Silkin, B. Hellsing, S. Crampin, and P. M. Echenique, Phys. Rev. B **68**, 195422 (2003).

[18] C. Corriol, V. M. Silkin, D. Sánchez-Portal, A. Arnau, E. V. Chulkov, P. M. Echenique, T. von Hofe, J. Kliewer, J. Kröger, and R. Berndt, Phys. Rev. Lett. **95**, 176802 (2005).

[19] V. Chis, S. Caravati, G. Butti, M. I. Trioni, P. Cabrera-Sanfelix, A. Arnau, and B. Hellsing, Phys. Rev. B **76**, 153404 (2007).

[20] S. Eremeev, I. Sklyadneva, P. Echenique, S. Borisova, G. Benedek, G. Rusina, and E. Chulkov, Surf. Sci. **601**, 4553 (2007).

[21] S. V. Eremeev, G. G. Rusina, S. D. Borisova, and E. V. Chulkov, Fiz. Tverd. Tela (St. Petersburg) **50**, 311 (2008) [Phys. Solid State **50**, 323 (2008)].

[22] E. Wimmer, J. Phys. F: Met. Phys. **13**, 2313 (1983).

[23] T. Valla, M. Kralj, A. Šiber, M. Milun, P. Pervan, P. D. Johnson, and D. P. Woodruff, J. Phys.: Condens. Matter **12**, L477 (2000).

[24] D. A. Luh, T. Miller, J. J. Paggel, and T. C. Chiang, Phys. Rev. Lett. **88**, 256802 (2002).

[25] Y.-M. Chang, L. Xu, and H. W. K. Tom, Phys. Rev. Lett. **78**, 4649 (1997).

[26] A. Melnikov, I. Radu, U. Bovensiepen, O. Krupin, K. Starke, E. Matthias, and M. Wolf, Phys. Rev. Lett. **91**, 227403 (2003).

[27] Y. Matsumoto and K. Watanabe, Chem. Rev. (Washington, D.C.) **106**, 4234 (2006).

[28] K. Watanabe, N. Takagi, and Y. Matsumoto, Chem. Phys. Lett. **366**, 606 (2002).

[29] K. Watanabe, N. Takagi, and Y. Matsumoto, Phys. Rev. Lett. **92**, 057401 (2004).

[30] K. Watanabe, N. Takagi, and Y. Matsumoto, Phys. Rev. B **71**, 085414 (2005).

[31] Y. Matsumoto, K. Watanabe, and N. Takagi, Surf. Sci. **593**, 110 (2005).

[32] K. Watanabe, N. Takagi, and Y. Matsumoto, Phys. Chem. Chem. Phys. **7**, 2697 (2005).

[33] M. Fuyuki, K. Watanabe, and Y. Matsumoto, Phys. Rev. B **74**, 195412 (2006).

[34] M. Fuyuki, K. Watanabe, D. Ino, H. Petek, and Y. Matsumoto, Phys. Rev. B **76**, 115427 (2007).

[35] D. Tang, D. McIlroy, X. Shi, and D. Heskett, Surf. Sci. Lett. **255**, L497 (1991).

[36] S. D. Borisova, G. G. Rusina, S. V. Eremeev, G. Benedek, P. M. Echenique, I. Y. Sklyadneva, and E. V. Chulkov, Phys. Rev. B **74**, 165412 (2006).

[37] W. C. Fan and A. Ignatiev, Phys. Rev. B **37**, 5274 (1988).

[38] M. D. Segall, P. J. D. Lindan, M. J. Probert, C. J. Pickard, P. J. Hasnip, S. J. Clark, and M. C. Payne, J. Phys.: Condens. Matter **14**, 2717 (2002).

[39] S. J. Clark, M. D. Segall, C. J. Pickard, P. J. Hasnip, M. J. Probert, K. Refson, and M. C. Payne, Z. Kristallogr. **220**, 567 (2005).

[40] K. Laasonen, A. Pasquarello, R. Car, C. Lee, and D. Vanderbilt, Phys. Rev. B **47**, 10142 (1993).

[41] J. P. Perdew, K. Burke, and M. Ernzerhof, Phys. Rev. Lett. **77**, 3865 (1996).

[42] H. J. Monkhorst and J. D. Pack, Phys. Rev. B **13**, 5188 (1976).

[43] S.-Å. Lindgren and L. Walldén, Phys. Rev. B **45**, 6345 (1992).

[44] R. W. Verhoef, W. Zhao, and M. Asscher, J. Chem. Phys. **106**, 9353 (1997).

[45] S. Reiff, W. Drachsel, and J. H. Block, Surf. Sci. **304**, L420 (1994).

[46] H. W. K. Tom, C. M. Mate, X. D. Zhu, J. E. Crowell, T. F. Heinz, G. A. Somorjai, and Y. R. Shen, Phys. Rev. Lett. **52**, 348 (1984).

[47] T. Luce, W. Hübner, and K. Bennemann, Z. Phys. B: Condens. Matter **102**, 223 (1997).

[48] J. Hohlfeld, S. S. Wellershoff, J. Güdde, U. Conrad, V. Jähnke, and E. Matthias, Chem. Phys. **251**, 237 (2000).

[49] Y.-M. Chang, L. Xu, and H. K. Tom, Chem. Phys. **251**, 283 (2000).

[50] A. E. Johnson and A. B. Myers, J. Chem. Phys. **104**, 2497 (1996).

[51] S.-Å. Lindgren, C. Svensson, and L. Walldén, J. Electron Spectrosc. Relat. Phenom. **64-65**, 483 (1993).

[52] C. Astaldi, P. Rudolf, and S. Modesti, Solid State Commun. **75**, 847 (1990).

[53] P. He and K. Jacobi, Phys. Rev. B **53**, 3658 (1996).

[54] C. Klünker, C. Steimer, J. B. Hannon, M. Giesen, and H. Ibach, Surf. Sci. **420**, 25 (1999).

[55] L. Padilla-Campos and A. Toro-Labbé, J. Chem. Phys. **108**, 6458 (1998).

[56] B. N. J. Persson, E. Tosatti, D. Fuhrmann, G. Witte, and C. Wöll, Phys. Rev. B **59**, 11777 (1999).

[57] B. N. J. Persson and J. W. Gadzuk, Surf. Sci. Lett. **410**, L779 (1998).

[58] T. A. Luce and K. H. Bennemann, Phys. Rev. B **58**, 15821 (1998).

[59] Z. C. Ying and W. Ho, J. Chem. Phys. **93**, 9089 (1990).

[60] *Handbook of Optical Constants of Solids*, edited by E. D. Palik (Academic, Orlando, 1985).

[61] R. Merlin, Solid State Commun. **102**, 207 (1997).

[62] The instantaneous response resembles a coherent spike often observed in conventional pump-probe spectroscopy, where pump and probe pulses are derived from a same light source. Since the center wavelengths of pump (565 nm) and probe (800 nm) pulses are well separated in the current measurements, the coherent coupling is not responsible for the negative component.